NRL Memorandum Report 5756

Near-Surface Bubble Motions in Sea Water

E. W. MINER AND O. M. GRIFFIN
Fluid Dynamics Branch
Marine Technology Division

R. A. SKOP
Rosenstiel School of Marine and Atmospheric Sciences
University of Miami

March 31, 1986

NAVAL RESEARCH LABORATORY
Washington, D.C.

AD-A168 395

SECURITY CLASSIFICATION OF THIS PAGE

REPORT DOCUMENTATION PAGE

1a. REPORT SECURITY CLASSIFICATION UNCLASSIFIED	1b. RESTRICTIVE MARKINGS
2a. SECURITY CLASSIFICATION AUTHORITY	3 DISTRIBUTION / AVAILABILITY OF REPORT *Approved for public release; distribution unlimited.*
2b. DECLASSIFICATION / DOWNGRADING SCHEDULE	
4. PERFORMING ORGANIZATION REPORT NUMBER(S) NRL Memorandum Report 5756	5 MONITORING ORGANIZATION REPORT NUMBER(S)
6a. NAME OF PERFORMING ORGANIZATION Naval Research Laboratory 6b OFFICE SYMBOL *(If applicable)* 5841	7a. NAME OF MONITORING ORGANIZATION Office of Naval Research
6c. ADDRESS (*City, State, and ZIP Code*) Washington, DC 20375-5000	7b. ADDRESS (*City, State, and ZIP Code*) Arlington, VA 22217
8a. NAME OF FUNDING / SPONSORING ORGANIZATION Office of Naval Research 8b. OFFICE SYMBOL *(If applicable)*	9. PROCUREMENT INSTRUMENT IDENTIFICATION NUMBER
8c. ADDRESS (*City, State, and ZIP Code*) Arlington, VA 22217	10 SOURCE OF FUNDING NUMBERS PROGRAM ELEMENT NO: 61153N; PROJECT NO:; TASK NO: RR023-01041; WORK UNIT ACCESSION NO: DN380-021

11 TITLE (*Include Security Classification*)

Near-Surface Bubble Motions in Seawater

12 PERSONAL AUTHOR(S)

Miner, E.W., Griffin, O.M., and Skop, R.A.

13a. TYPE OF REPORT	13b. TIME COVERED	14. DATE OF REPORT (*Year, Month, Day*)	15 PAGE COUNT
Interim	FROM 10/84 TO 11/85	1986 March 31	31

16 SUPPLEMENTARY NOTATION

17 COSATI CODES			18 SUBJECT TERMS (*Continue on reverse if necessary and identify by block number*)
FIELD	GROUP	SUB-GROUP	Bubbles, Bubble Transport, Wakes, Ship Wakes, Surface Foam, Numerical Methods

19 ABSTRACT (*Continue on reverse if necessary and identify by block number*)

This report considers one aspect of the problems associated with bubbles in the wake of a surface ship. A method which has been developed for calculating the evolution and transport of bubbles is described. Results which were obtained with this method are presented and are compared with the limited experimental data which is available. Generally good agreement was found between the numerical and experimental results. Several areas are noted where further research is indicated.

20 DISTRIBUTION / AVAILABILITY OF ABSTRACT	21 ABSTRACT SECURITY CLASSIFICATION
☒ UNCLASSIFIED/UNLIMITED ☐ SAME AS RPT ☐ DTIC USERS	UNCLASSIFIED
22a NAME OF RESPONSIBLE INDIVIDUAL E.W. Miner	22b TELEPHONE (*Include Area Code*) 202-767-3389
	22c OFFICE SYMBOL Code 5841

DD FORM 1473, 84 MAR 83 APR edition may be used until exhausted
All other editions are obsolete

SECURITY CLASSIFICATION OF THIS PAGE

CONTENTS

NEAR-SURFACE BUBBLE MOTIONS IN SEA WATER

INTRODUCTION

The acoustic wake of a surface ship is almost exclusively that part of the overall hydrodynamic wake which contains surface and underwater bubbles. The bubbles are produced when the ship's propellors entrain air from the surface region and when air is entrained into the hull boundary layer. Additional sources of bubbles are propellor cavitation and breaking of the ship's bow wave. The bubbles which emanate into the far-field wake from the vicinity of the ship also contribute to the visible surface foam layer when they rise from the underwater wake region. The acoustic effect of the bubbles arises when they resonate at particular frequencies which are determined principally by the bubbles' diameters. Then acoustic energy is absorbed and scattered at the resonant frequencies of the wake bubble population.

A comprehensive prediction model for the acoustic or bubble wake of a surface ship should include such ship characteristics as the displacement, length, beam and draft. The location, geometry and operational parameters of the ship's propellors also are required. Environmental parameters to be considered include the sea state and the temperature, salinity and density distributions in the ambient ocean. The development of a model which includes all of these parameters is a formidable task. This report considers just one aspect of a comprehensive model of the bubble wake; that is, a method which has been developed for calculating the evolution and transport of bubbles in a wake.

THE NUMERICAL METHOD

In the region close to the ship, the bubble wake cannot be calculated. The complexity of this region is discussed by Skop (1984) and is clearly seen in Figure 1 which is taken from Peltzer (1984). This figure also clearly shows the three separate sources of bubble generation. As the bow wave folds over, air is entrained into the flow in a manner quite similar to the generation of subsurface bubbles by wind-driven breaking waves (Thorpe, 1982). Additional bubbles and foam are generated as air is entrained into the flow by the turbulent boundary layer along the sides of the hull. The propeller wake can be divided into two regions, an initial region of high divergence directly behind the stern called the initial spreading region and the far wake where the wake spreads at a small angle of about one degree.

Manuscript approved January 1, 1986.

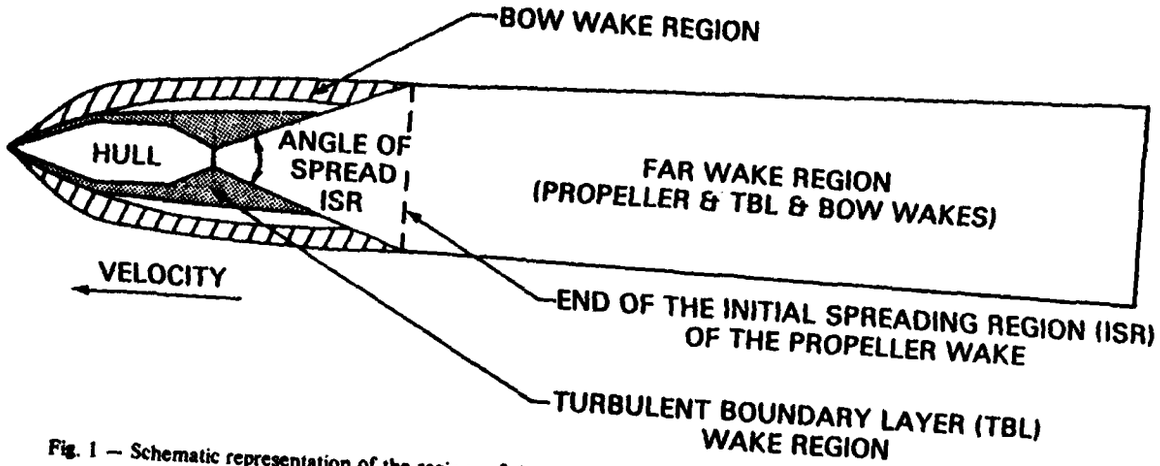

Fig. 1 — Schematic representation of the regions of the "white water" wake of a surface vessel; from Peltzer (1984).

The bow wake and the turbulent boundary layer wake regions both merge with the propeller wake in the initial spreading region.

The parameters of the initial spreading region for the case of a destroyer are shown in Figure 2 which is adapted from work performed at the Naval Ocean Systems Center and which is based on the results presented in NDRC (1946). Clearly, for different vessels, the parameters of the initial spreading region will change significantly based upon propeller diameter, r.p.m. and submergence, upon vessel speed, geometry and resistance and upon many other factors. In the so called "far wake," the flow field is much more regular and amenable to solution by numerical means. Thus, the end of the initial spreading region is an appropriate point to begin calculations for the acoustic wake. Calculations of the acoustic wake would in general use some of the results obtained for the hydrodynamic wake, such as the velocity components in the different directions for calculating bubble transport. However, other methods must be utilized for determining the evolution of individual bubbles or ensembles of bubbles.

The discussion of multiphase flows given by Skop (1984) provides a useful starting point in a development of a model of the dynamics of bubbles in the acoustic wake. Garrettson (1973) has taken a somewhat different approach and has developed a general transport equation for a bubble distribution as a function of position, velocity, bubble radius and time. Garrettson also developed a procedure for integrating the transport equation including any distributed sources and sinks along the characteristic curves of the bubbles. For the one-dimensional, steady-state ocean example which he considers, the characteristic curves are vertical straight lines. Elimination of distributed sources simplifies the situation still further.

Such a solution procedure corresponds quite closely to calculating the trajectories of groups of individual bubbles and assigning an appropriate number count to the various trajectories. The latter approach was chosen in the present case since an existing multi-component gas bubble dynamics code was already available. That code was based on work done under contract for the Naval Ocean Systems Center in that the trajectories of a group of bubbles are calculated in position, bubble radius and time. With some adjustments in either the code or in the input data, the gas in the bubble may be single component or an interaction between multiple components. For the individual bubbles the governing equation is

$$\frac{dM}{dt} = AW(C_a - C_s)$$

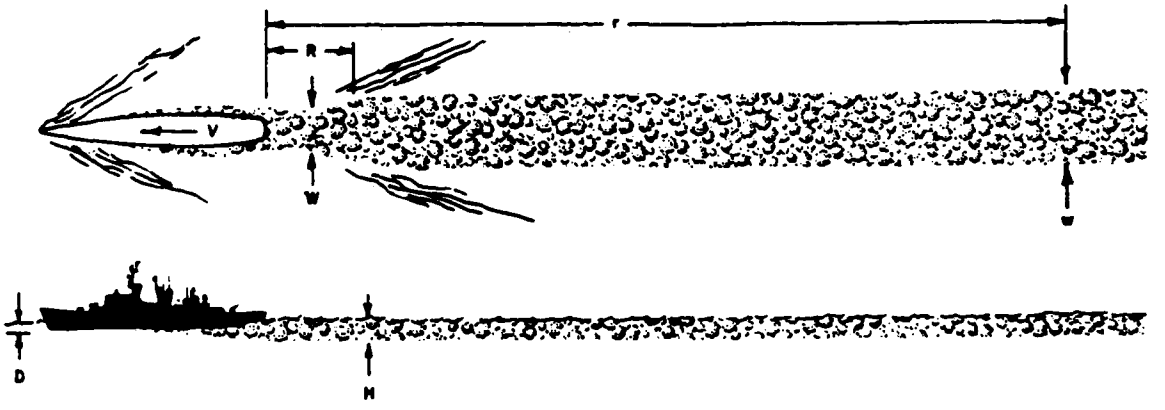

H = ∿ 2D
H CONSTANT FOR r UP TO 1000 YDS
FOR R ≤ 100 YDS OR LESS
DEPENDING UPON V:

V(Kn)	R(YD)	W(YD)
16	21	18
20	39	35
25	75	64
33	93	80

FOR r ≥ 100 YDS OR MORE:
w = W + .017 (r − R)

V = VELOCITY OF SHIP IN KNOTS
H = DEPTH OF WAKE IN FEET
D = DRAFT OF VESSEL IN FEET
R = DISTANCE ASTERN (100 YDS OR LESS)
W = WIDTH OF WAKE IN YDS UP TO MAX. R
r = DISTANCE ASTERN (100 YDS OR MORE)
w = WIDTH OF WAKE IN YARDS

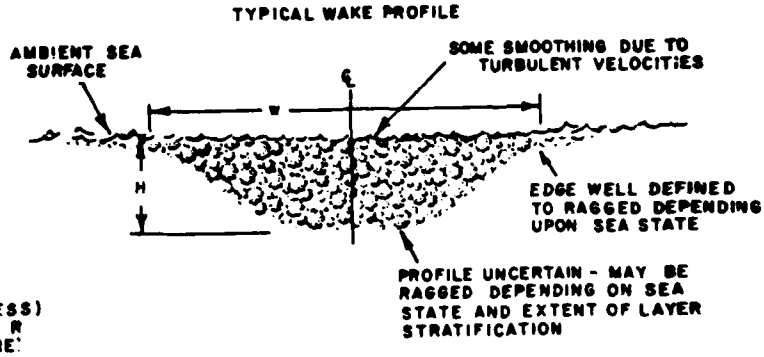

Fig. 2 — Predicted wake of a destroyer based on NDRC (1946)

where $\frac{dM}{dt}$ is the rate of mass transfer to or from the bubble in micro-moles per second (μ moles/sec), A is the surface area of the bubble, W is the mass transfer coefficient at the bubble surface, C_a is the concentration of the dissolved gas or gases in the surrounding ambient fluid (μ moles/cm^3) and C_s is the concentration of the dissolved gas in the bubble skin (μ moles/cm^3). Henry's law of gas solubility is used to determine the skin concentration, giving

$$C_s = GP$$

where G is the solubility coefficient (μ moles/(cm^3 · atm)) and P is the partial pressure of the gas (atm) which is assumed to be in equilibrium with the surrounding fluid.

The mass transfer coefficient which is used depends on the gas-to-liquid diffusivity, density and viscosity as well as how the transfer of gas to or from the bubble takes place. Very small bubbles seem to have a steady state concentration profile established in the surface film layer whereas larger bubbles rise rapidly enough that a steady state concentration profile is not established. Accordingly, and following Jeter, the mass transfer coefficients, W (cm/sec) are given by

$$W = 2\sqrt{\frac{D_i V}{\pi D}} \; ; \; D > 0.3\text{cm}$$

$$= D\frac{1.13}{0.3}\sqrt{D_i \frac{25.25}{0.3}} \; ; \; 0.06 < D \leqslant 0.3\text{cm}$$

$$= 0.31\left(\frac{\mu g}{\rho}\right)^{1/3}\left(\frac{\mu}{\rho D_i}\right)^{-2/3} \; ; \; D \leqslant 0.06\text{cm}$$

where V is the bubble velocity (cm/sec), D is the diameter (cm), μ and ρ are the fluid viscosity (gm/cm/sec) and density (gm/cm^3) and D_i is the molecular diffusivity (cm^2/sec) of the ith gas component.

The mass transfer equation is applied separately for each gas in the bubble. The various gases interact only in that the presence of one affects the partial pressure of another and the total size of the bubble. The partial pressures of the gas components are additive following Dalton's law and the ideal gas law provides the equation of state for the gases and a means for calculating the bubble volume. At all times, the bubble is assumed to contain enough water vapor so that the partial pressure of the water vapor is equal to vapor pressure of the surrounding sea water.

In order to use the bubble dynamics code, appropriate values for the concentrations, molecular diffusivities and solubilities are needed. In the most complete version of the model that was used,

values were needed for hydrogen, nitrogen, oxygen and carbon dioxide. The values of solubility G for an assumed temperature of 25 C were taken from Weast (1965) and are given below:

GAS	G	
	$l/(l \cdot \text{atm})$	moles/$(l \cdot \text{atm})$
H_2	0.0175	0.000716
N_2	0.0143	0.000585
O_2	0.0283	0.001156
CO_2	0.759	0.0310

The values of solubility for O_2 and N_2 given above were compared with values from Horne (1969) for solubility in water with various amounts of dissolved chlorine and satisfactory agreement was found. The molecular diffusivities, D_i at 25 C were obtained from Perry and Chilton (1979) and follow:

GAS	D_i (cm^2/s)
H_2	5.85×10^{-5}
N_2	1.9×10^{-5}
O_2	2.5×10^{-5}
CO_2	1.96×10^{-5}

Horne (1969) gives similar values for N_2 and O_2 at 20 C and for pure water.

Gaseous concentrations, C_a, in seawater are quite variable depending upon both location and temperature. The values of concentration that were used in the initial calculations with the bubble dynamics code were found in Harvey (1960) and were as listed below:

GAS	C_a (ml/l)
H_2	2.0×10^{-4}
N_2	9.05
O_2	5.0
CO_2	0.129

To match the available data for solubilities and diffusivity, the temperature was taken to be 25 C and the corresponding water vapor pressure is 23.76 mm Hg.

DISCUSSION OF RESULTS

For the study of bubbles in the wake of a ship, there is little data with which to work. *Physics of Sound in the Sea* (NDRC 1946) contains some data on the attenuation of sonar signals across the wake made by a destroyer at 15 knots. Measurements were made at four frequencies and at one, three and five minutes after the ship passed. These data are given in Table I.

The volume of air per cm^3 for bubbles in resonance with the sonar signal as calculated from the measurements of the attenuation of the sonar signals is also given in NDRC (1946). The corresponding bubble number density (N, per 10 cm^3) is given in Table II, and plotted in Fig. 3. The curves which are drawn through the data points are based on the assumption that the peak value of N occurs at a diameter of about 80 microns and is only a small amount (20 to 40%) greater than the value of N at $D = 160\ \mu m$. It was also assumed that N would have a positive value as $D \rightarrow 0$. These two assumptions influence the shapes of the curves for $D > 160\mu m$. The assumption that the peak value of N occurs at about 80 μm is based on the work of Thorpe (1982) and Garrettson (1973) and the results obtained by Johnson and Cooke (1979) for bubbles under breaking waves. The portion of these faired curves from 160 μm to 400 μm is shown in Fig. 3.

Initial bubble distributions in the present work were based on the curve for 1 min and comparisons were made with the 3 and 5 min curves shown in Fig. 3. In addition to the uncertainty of what the bubble density curves should look like between 160 and 320 μm, there is the question of how the bubble density should vary with depth. It is assumed that the 1 min curves apply at any depth when multiplied by an appropriate factor. The simplest distribution with depth would be constant for the depth of the wake. The depth of the wake was assumed to be 8 m (corresponding to the wake depth for destroyers as given in NDRC - 1946). The distribution of N with depth was given a slight rounding at 7, 8, 10 and 11 m as shown in Fig. 4. As will be seen later, the rounding of the initial depth distribution curve at 7 and 8 m leads to a slight difference between the numerical and experimental curves for the depth-averaged number density distribution at $t = 1$ min.

Calculations were first made with the density distribution as described above and for a gas mixture of oxygen, nitrogen, carbon dioxide and water vapor in the bubble and for the corresponding gases dissolved in the seawater. The chemical constants used were those described earlier. In the preliminary calculations, several problems arose. The inclusion of CO_2 led to a strong instability in the smaller bubbles and required a greatly reduced time step. A series of tests showed that the CO_2 could be omitted without compromising the validity of the calculations. Further, the work of Thorpe (1982) and Garrettson (1973) had earlier suggested that a multi-component gas bubble could be approximated very

Table I — Attenuation Coefficient and Density of Resonant Bubbles—Destroyer at 15 knots (NDRC 1946)

Frequency in kHz	Age of wake and distance astern						R_r in cm
	1 minute 500 yd astern		3 minutes 1,500 yd astern		5 minutes 2,500 yd astern		
	K_e	$u(R_r)$	K_e	$u(R_r)$	K_e	$u(R_r)$	
3	0.35	2.5×10^{-6}	0.03	2.1×10^{-7}	...	...	0.107
8	0.67	4.8×10^{-6}	0.21	1.5×10^{-6}	0.03	2.1×10^{-7}	0.040
20	1.11	7.9×10^{-6}	0.48	3.4×10^{-6}	0.22	1.6×10^{-6}	0.016
40	1.65	1.18×10^{-5}	0.79	5.6×10^{-6}	0.43	3.1×10^{-6}	0.008

Notes:

1. R_r is the resonance radius of the bubble.
2. $u(R_r)$ is the volume fraction of air for bubbles of that radius.
3. K_e is the attenuation coefficient in decibels per yard.

Table II — Bubble Number Density — N/(10 cm^3)

R_r cm	D_r microns	Age of wake		
		1 minute	3 minutes	5 minutes
0.107	2140	4.9×10^{-3}	4.1×10^{-4}	—
0.040	800	0.179	0.056	7.8×10^{-3}
0.016	320	4.6	1.98	0.93
0.008	160	55	26.1	14.5

Notes

1. R_r is the resonance radius of bubbles.
2. D_r is the resonance diameter of bubbles.

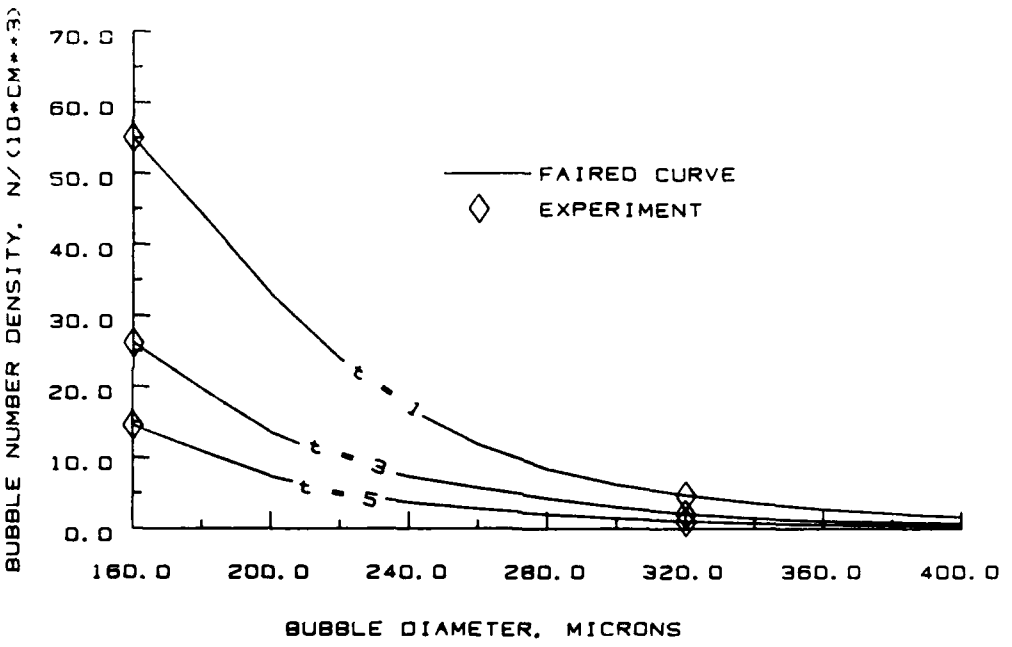

Fig. 3 — Curves as faired through experimental data of NDRC (1946)

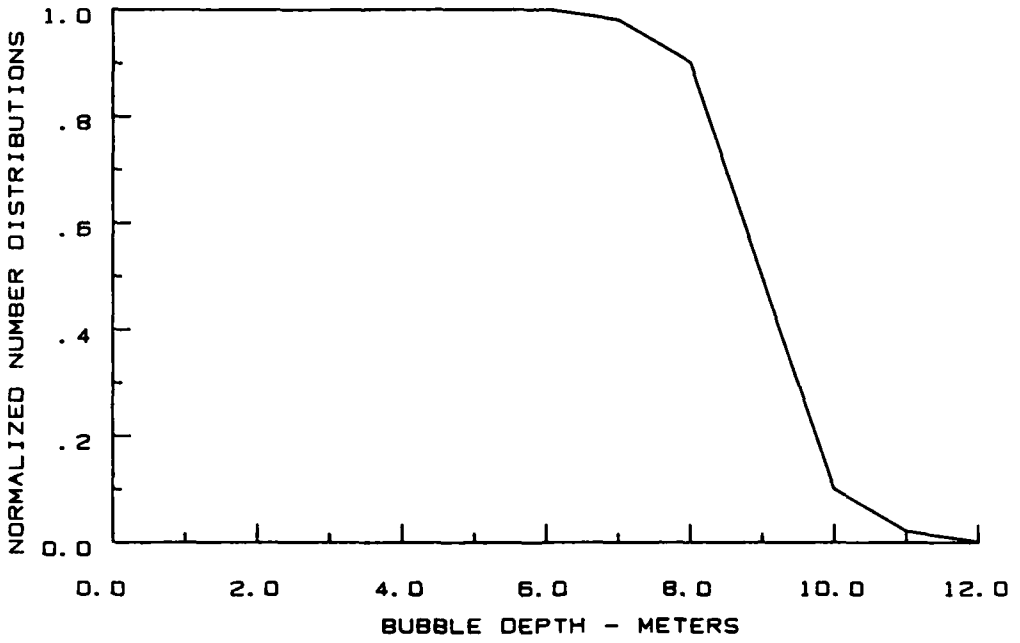

Fig. 4 — Variation of bubble number density with depth as used for the t = 1 min data

well by a bubble composed of only nitrogen. Additional test calculations are made for nitrogen only bubbles over a range of diameters and depths. The results of these calculations supported the premise that a nitrogen only model could be substituted for a full multi-component gas model for most purposes. Such a simplification of the bubble chemistry not only reduces the number of calculations required per time step, but also it allows the use of a larger time step in the calculations. This is most advantageous when numerous developmental calculations are being made.

An additional observation was made during the course of these calculations. This was the short life of the wake. By this is meant that very few of the bubbles would last beyond ten minutes and certainly not for upwards of the thirty minutes that is suggested for wake persistence in NDRC (1946). Several factors were considered that might extend the lifetimes of the bubbles. The first factor was adding a downwash velocity to the calculations to simulate the swirl in the flowfield induced by the bow wave and by the ship's propellers. It was determined that a down-wash velocity in the range of 0.5 to 2.0 cm/s increased the time that some bubbles would last, but only by a factor of about one-fourth. With the inclusion of a downwash, more of the small bubbles were being completely dissolved and more of the intermediate-sized bubbles were being reduced in size. That is, fewer bubbles were rising to the surface (a desired effect) but the other bubbles were being dissolved to a greater extent than when a downwash was not imposed.

The next factor considered was the concentration of nitrogen in the sea water. The calculations thus far had been made with $C_N = 9.0$ *ml/l* which, as noted above, is an appropriate estimate of the amount of dissolved nitrogen in seawater. However, for a nitrogen-only bubble, this value of C_N was low and the smallest bubbles included in the calculation (20 μm) were still being dissolved well before they reached the surface. It was decided to increase C_N to better simulate saturation of nitrogen at the upper levels of the sea. Figure 5 shows the results of this change in C_N. The non-dimensionalized bubble volume (bubble volume divided by bubble volume at time of release) is shown for eight bubbles released at 1 m depth and also at 3 m. The bubble diameters were 80, 120, 160, 180, 200, 240, 280 and 320 μm. For this new value of C_N (13.5 *ml/l*) the smaller bubbles appear to be in equilibrium (neither gaining or losing volume) at about 0.7 m depth. This seems to be a reasonable approximation of a saturated surface layer and $C_N = 13.5$ *ml/l* was used in the remainder of the nitrogen only calculations.

Calculations were made for these conditions and the results are shown in Figs. 6-8. Figure 6 shows the number density (N = number/10cm^3) contours in the initial plane ($t = 1$ min). These initial contours were used in all subsequent calculations. The vertical axis is the bubble diameter in microns (μm) and the horizontal axis is depth in meters. The accented contour curves are for intervals of 10 in N and the lighter contours are for intervals of 2. This figure clearly shows (for each diameter) a nearly

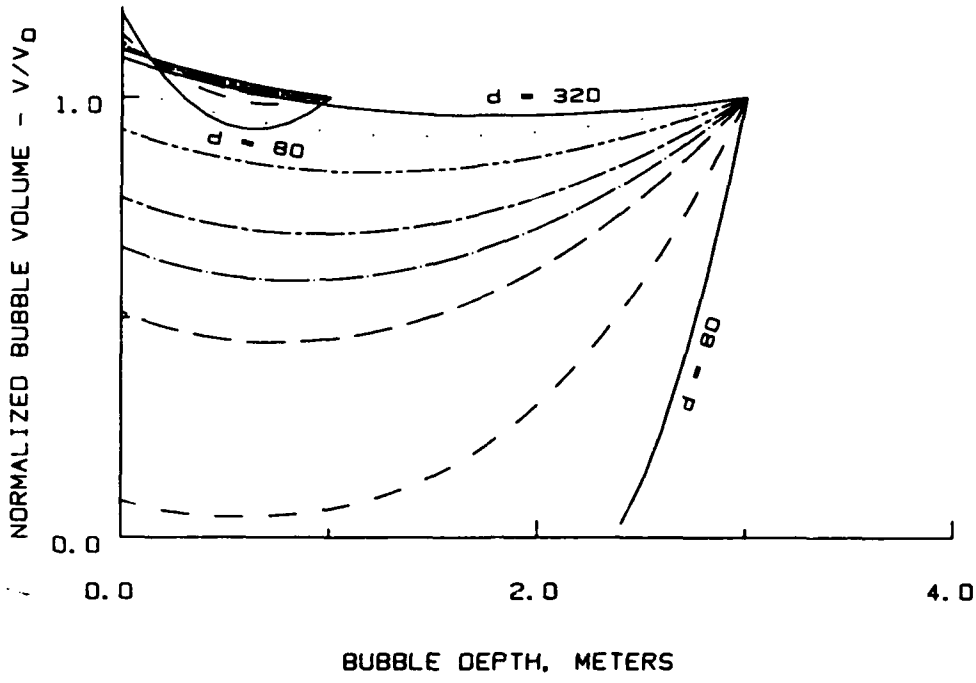

Fig. 5 — Curves of normalized volume V_n vs depth D for N_2 bubbles of diameters 80 to 320 microns showing surface layer saturation

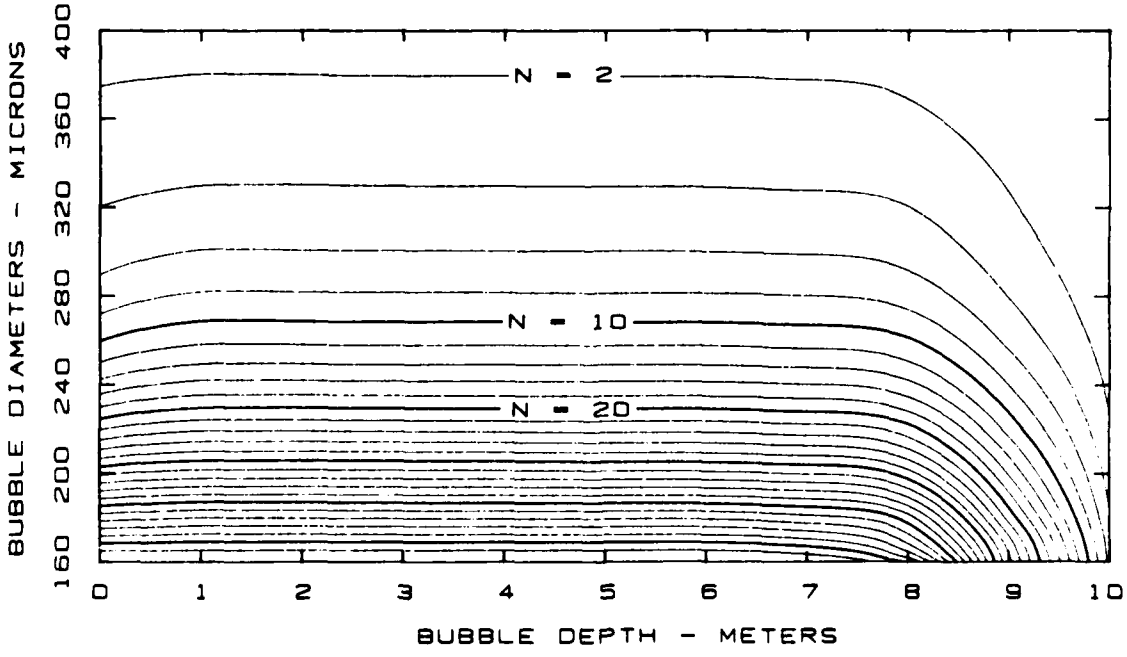

Fig. 6 — Initial (t = 1 min) number density N (number/(10 cm**3)) contours as as a function of D and Z

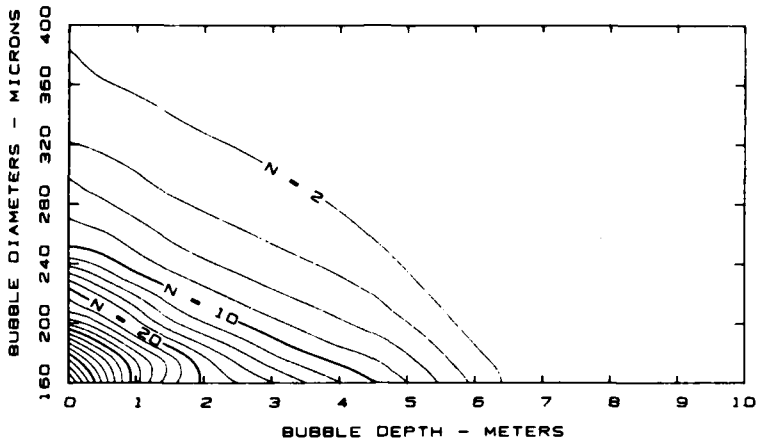

(a)

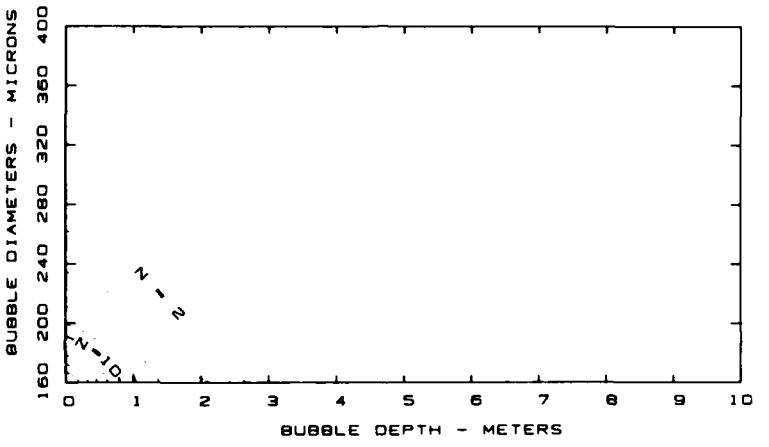

(b)

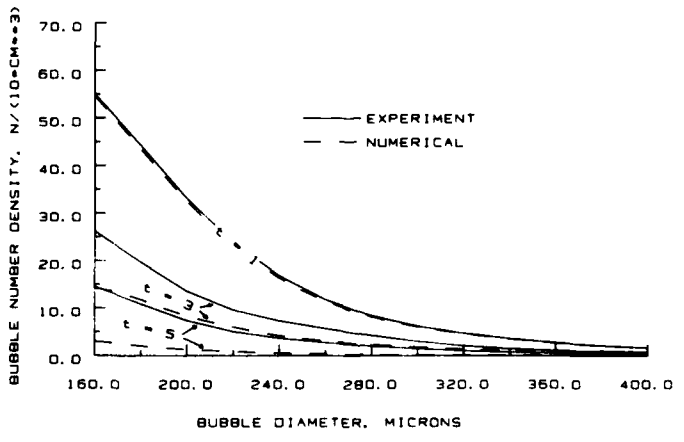

(c)

Fig. 7 — Number density distributions with "clean" bubble or standard diffusivity: (a) as a function of D and Z at $t = 3$ min, (b) as a function of D and Z at $t = 5$ min, and (c) depth averages for times $t = 1, 3, 5$ min

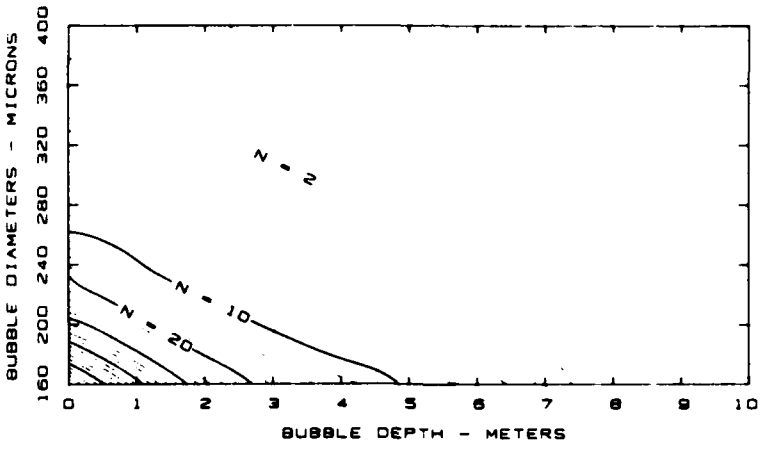

(a)

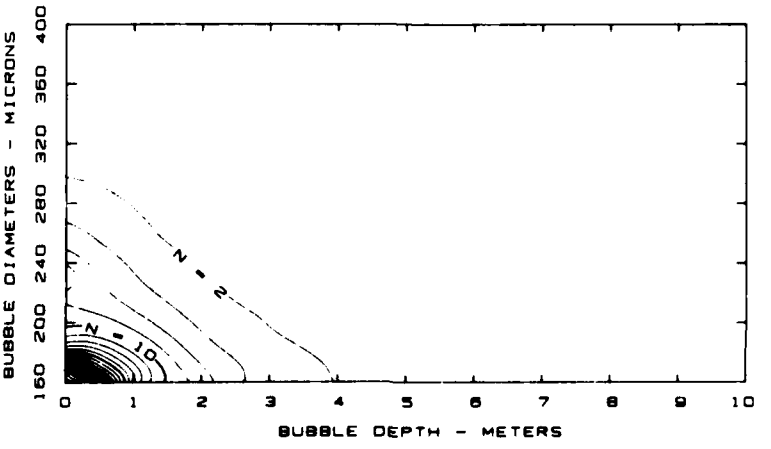

(b)

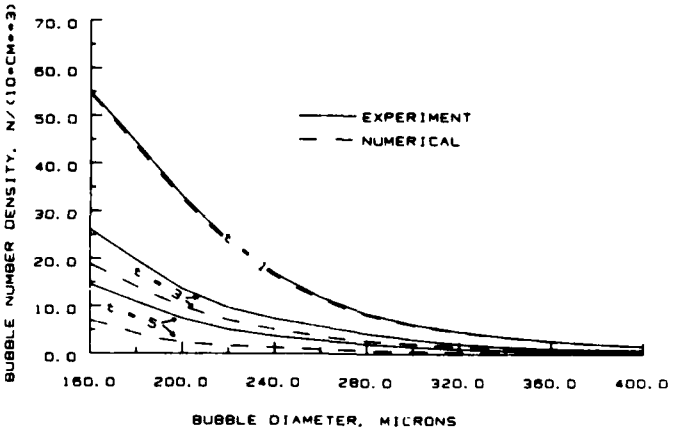

(c)

Fig. 8 — Number density distributions with "clean" bubble or standard diffusivity and 1 cm/s downwash: (a) as a function of D and Z at $t = 3$ min, (b) as a function of D and Z at $t = 5$ min, and (c) depth averages for times $t = 1, 3, 5$ min

constant distribution with depth to 8 m and then a linear decrease to almost zero by 11 m. If only the upper 8 m of the number density distribution are included in a depth average, the results match almost exactly the initial curve. The contour plots of N as a function of D and Z for $t = 3$ and 5 minutes are shown in Figs. 7a and 7b. Depth-averaged values of N are shown in Fig. 7c. These figures show quite a rapid decline with time in the population of bubbles with diameters of 160 μm or greater (i.e. in the experimental range). The depth-averaged values of N (averaged from 0 to 8 m) for $t = 1$, 3 and 5 minutes show better just how rapid that decline is; the slight discrepancy at 1 minute is due to rounding of the depth distribution curve at 8 m as noted above. Clearly these calculations greatly under predict the bubble population at both 3 and 5 minutes.

The amount by which the bubble population is under predicted at 3 and 5 minutes suggests that some part of the numerical simulation needs to be improved. The basic mechanics of the simulation seem to have been tested fully in the past. One characteristic of the flow field which was not simulated was the swirl given to the flow in a ship's wake by the propellers. Accurate inclusion of the swirl in the flow model would require not only a three-dimensional formulation but also an accurate knowledge of the swirling flow field. However, a reasonable indication of the effect of the swirl on the bubble population can be determined even with a two-dimensional formulation by the expedient of adding a small downwash velocity to the simulation. Since we are primarily interested in the effects at 3 and 5 minutes after the passage of the ship, we might well expect that most residual swirl velocities would be rather small.

The effect of a downwash velocity of 1 cm/s was considered and the results are shown in Fig. 8. The contours of bubble number density are shown in Fig. 8a for $t = 3$ and in Fig. 8b for $t = 5$ min. The depth-averaged values of N are shown in Fig. 8c. The addition of a 1 cm/s downwash does indeed reduce the rapidity of the bubble population decline but the agreement between experiment and simulation seen in Fig. 8c still needs to be improved. However, other calculations with either more or less downwash showed little improvement in the comparison. With greater downwash, bubbles are reduced in size more rapidly by the pressure increase and by the dissolution process. For less downwash than 1 cm/s, the results tended toward those shown in Fig. 7c.

Other factors in the simulation were considered as possible causes for the poor agreement between the experimental data and the results of the simulation. The values used for the bubble rise velocity were in agreement with those from many sources. Small differences did exist but would not have led to the size of the differences which we found. The value chosen for the solubility of nitrogen (or other gases in seawater) is somewhat uncertain since the solubility is affected significantly by the amount of chlorine in the seawater. However, differences in gas solubility will be mostly offset by

corresponding changes in the concentration of the gas. Any changes in solubility would require appropriate changes in concentration in order to approximate saturation in the near-surface layer. The principal remaining factor is the molecular diffusivity which controls the rate of gas transfer across the gas-liquid interface of the bubble surface. The value of diffusivity used in the calculations discussed above is perhaps more appropriate to processes in a chemical engineering reactor than to bubbles and foam in the open ocean. Specifically, the difficulty is that the value of diffusivity from Perry and Chilton (1973) is appropriate to "clean" bubbles in the way Garrettson (1973) and Thorpe (1982) use the term and probably inappropriate for "dirty" bubbles. In fact, it seems reasonable to assume (since appropriate experimental data is not available) that most of the bubbles in the wake of a ship rapidly acquire a coating of surface particles which slows the transfer of gas into or out of the bubble and also reduce its rise velocity.

The limiting case of reduced diffusivity is zero diffusivity which simulates a non-reacting gas with the bubble volume being proportional to the hydrostatic pressure. Calculations were made for zero diffusivity and the results are shown in Figs. 9 and 10. In these figures there is an obvious expansion of the bubbles as they rise (the number density increases) whereas in Figs. 7 and 8 the number density significantly decreases as the bubbles rise. This effect as seen in Figs. 7 and 8 is clearly due to the bubbles being dissolved by the seawater since for depths greater than 1 m the seawater is undersaturated (see Fig. 5) and most bubbles are partially dissolved as they rise. The depth-averaged number densities are given in Fig. 9c and show that the effect of diffusivity is quite important. These figures are for zero downwash and the results for a 1 cm/s downwash are given in Fig. 10. The combined effect of 1 cm/s downwash and no diffusivity is such that for $t = 3$ and 5 minutes the depth-averaged number density curves scarcely differ from the $t = 1$ minute curves. The inclusion of curves for $t = 7$, 8 and 9 minutes would show small but distinct differences.

The next results are for the "clean" bubble diffusivity reduced by a factor of one tenth. Even this limited amount of diffusion is enough to keep most of the bubbles from expanding except in the near-surface layer. The bubble number density distributions in Fig. 11 for $t = 3$ and 5 min and no downwash show that the primary process is dissolution of the bubbles. The depth averaged number density distributions in Figs. 11 and 12 indicate that this level of diffusivity is too low for an adequate match of the simulation results with the experimental results.

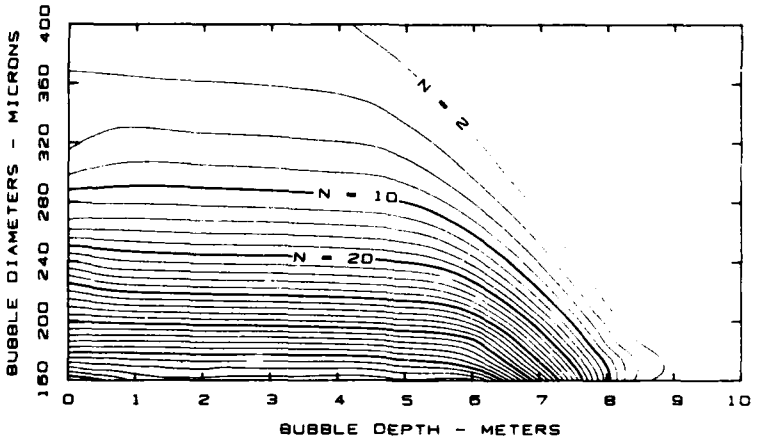

(a)

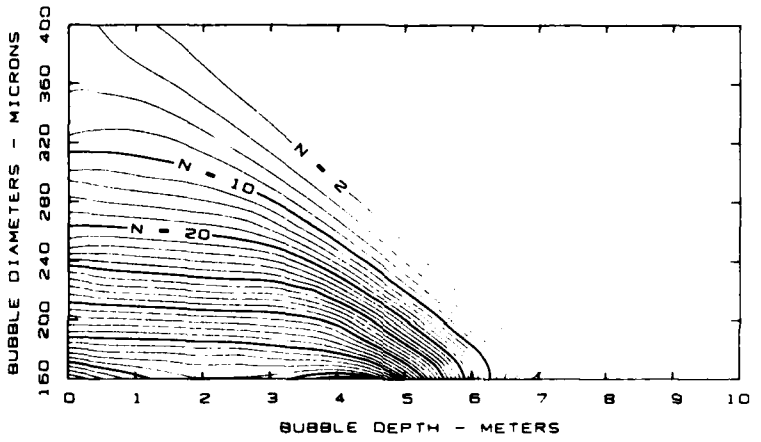

(b)

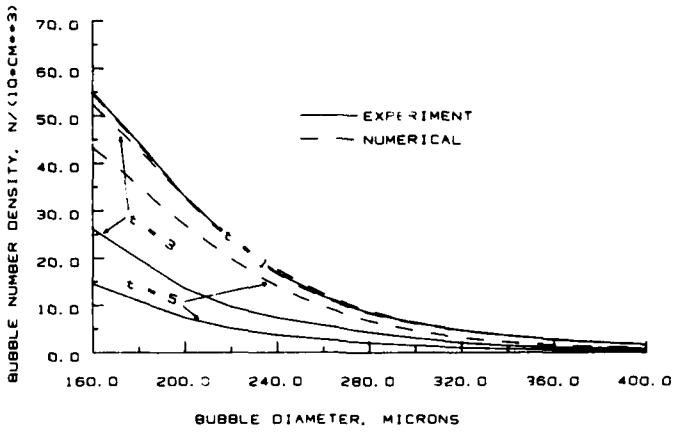

(c)

Fig. 9 — Number density distributions with zero diffusivity: (a) as a function of D and Z at $t = 3$ min, (b) as a function of D and Z at $t = 5$ min, and (c) depth averages for times $t = 1, 3, 5$ min

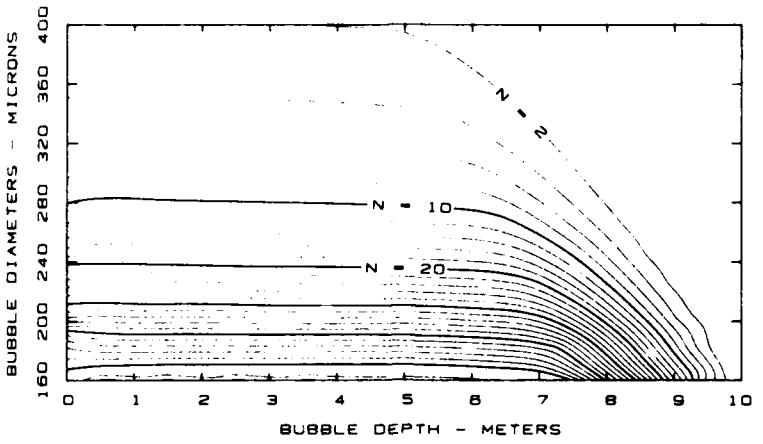

(a)

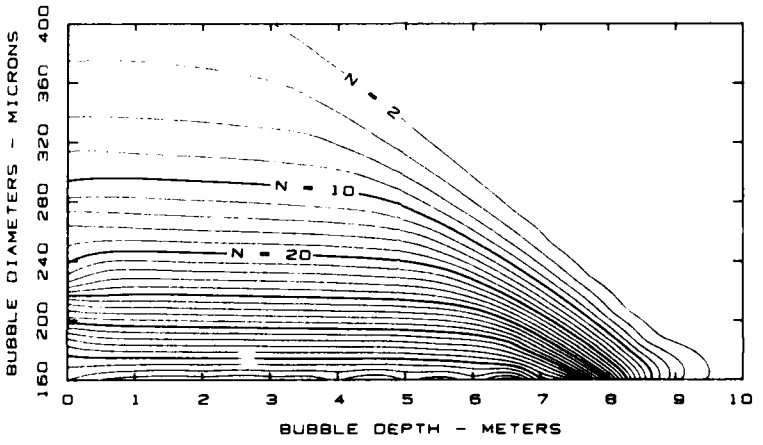

(b)

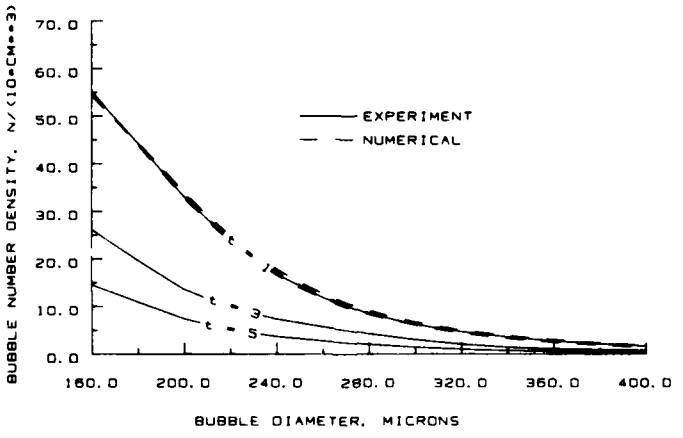

(c)

Fig. 10 — Number density distributions with zero diffusivity and 1 cm/s downwash: (a) as a function of D and Z at $t = 3$ min, (b) as a function of D and Z at $t = 5$ min, and (c) depth averages for times $t = 1, 3, 5$ min

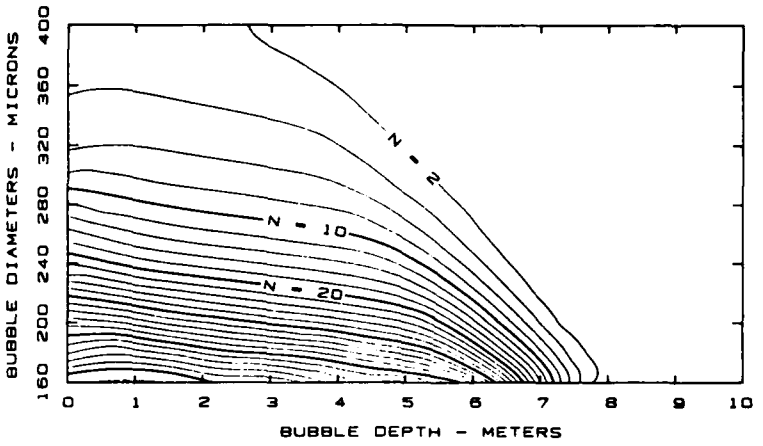

(a)

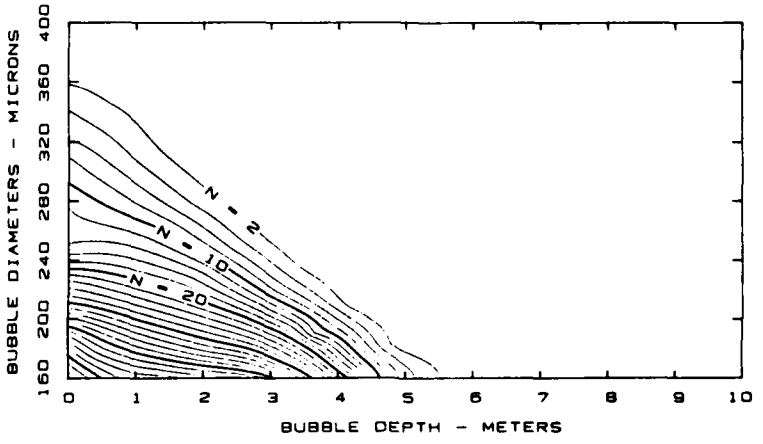

(b)

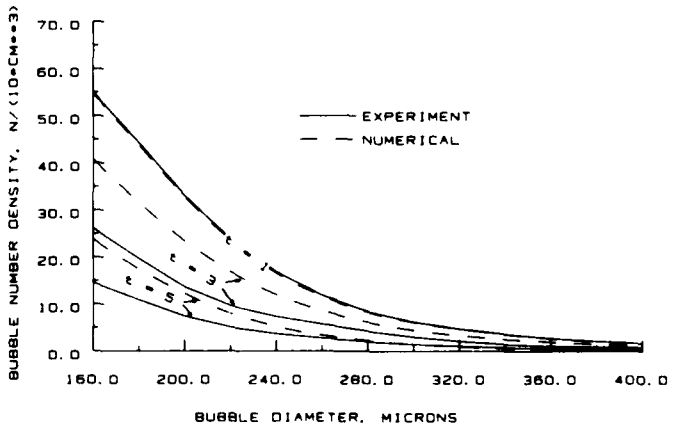

(c)

Fig. 11 — Number density distributions with standard diffusivity reduced by one tenth: (a) as a function of D and Z at $t = 3$ min, (b) as a function of D and Z at $t = 5$ min, and (c) depth averages for times $t = 1, 3, 5$ min

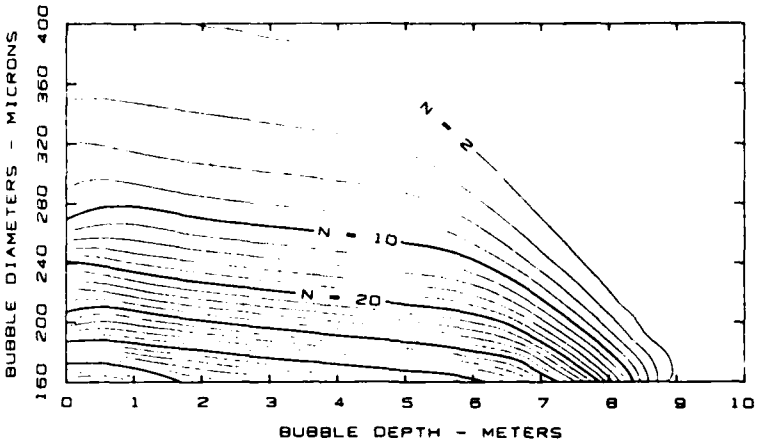

(a)

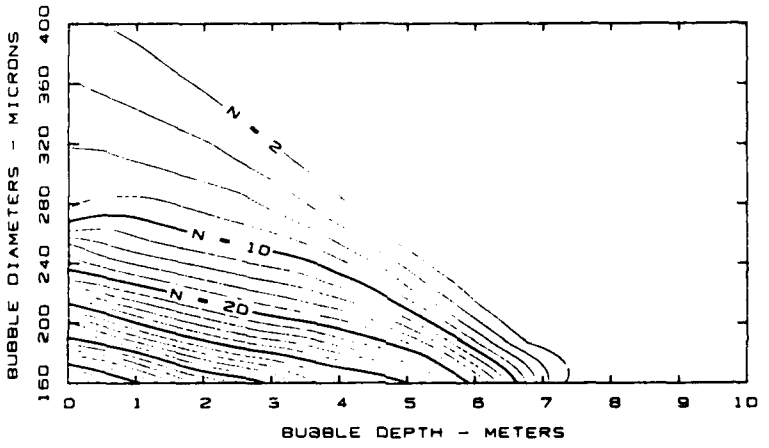

(b)

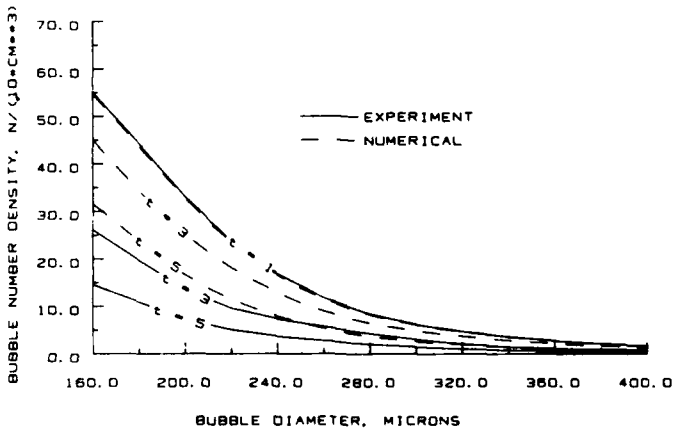

(c)

Fig. 12 — Number density distributions with standard diffusivity reduced by one tenth and with 1 cm/s downwash: (a) as a function of D and Z at $t = 3$ min, (b) as a function of D and Z at $t = 5$ min, and (c) depth averages for times $t = 1, 3, 5$ min

A much better match between the simulation results and the experimental data is obtained by using the "clean" bubble diffusivity reduced by one third. For this value of diffusivity the number density distributions are given in Figs. 13 and 14. The simulation results in these two figures reasonably match the experimental data. However, these particular calculations used the equations for the bubble rise velocity as given by Jeter (1974). The resulting bubble rise velocities appear to more closely match Thorpe's (1982) "clean" bubble values than his "dirty" bubble values, whereas a 20% reduction in the bubble rise solution would match fairly well the "dirty" bubble values of Thorpe. Results for the number densities using the reduced bubble rise velocities are shown in Figs. 15 and 16. With this change in the rise velocity together with the "clean" bubble diffusivity reduced by one third, the simulation results compare quite well with the experimental data, especially for the no downwash case. Since the changes in the molecular diffusivity of N_2 and the changes in the bubble rise velocities could have affected the assumptions that were made about the surface layer saturation, calculations were made for the test groups of bubbles in the surface layer. The results of these calculations (using "dirty" bubble rise velocities and standard diffusivity reduced by one third) are shown in Fig. 17. These curves do differ somewhat from the curves in Fig. 5 but not in a significant amount. The curves still show a saturation in the surface layer at about 0.7 m.

In the results presented above, the gas chemistry for the bubble was restricted to nitrogen-only (N_2) as discussed previously. Verification of the appropriateness of this limited gas model is obtained by repeating the last set of calculations (i.e., for a "dirty" bubble) for a more complex gas chemistry. When oxygen was added to the model, the equilibrium values of O_2 and N_2 needed to be adjusted in order to obtain bubble rise profiles comparable to those in Fig. 5. The values of CO_2 and CN_2 which gave matching bubble volume profiles were 5.5 and 10.5 *ml/l* respectively along with a diffusivity of one fourth of the standard bubble diffusivity. The bubble number density distributions for the $O_2 - N_2$ bubbles are given in Figs. 18 and 19. These number density distributions are quite similar to those in Figs. 15 and 16 for the N_2 only bubbles. The bubble volume profiles for the $O_2 - N_2$ bubbles with the adjusted diffusivities and concentrations and with "dirty" bubble rise velocities are shown in Fig. 20. The changes in chemistry, concentrations and diffusivities did change slightly the curves of bubble volume vs depth, but the curves still show a good approximation of saturation in the surface layer. A comparison of these results for the $O_2 - N_2$ bubbles (Figs. 18-20) with the comparable results for the N_2 only bubbles (Figs. 15-17) shows good agreement between the results of the two models and also good agreement between the simulation results and the experimental data.

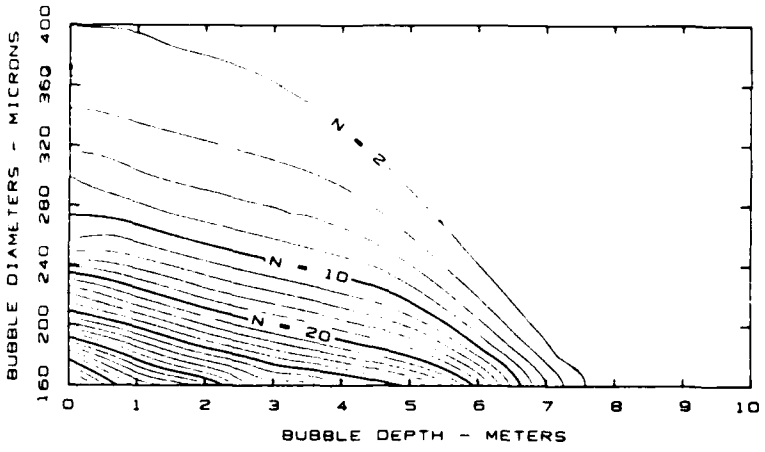

(a)

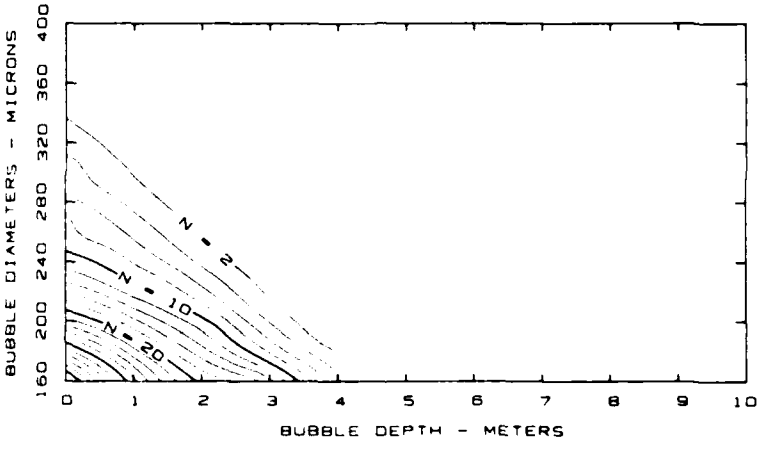

(b)

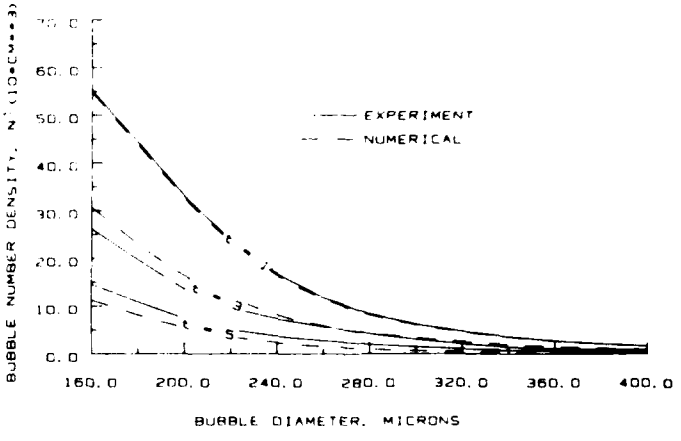

(c)

Fig. 13 — Number density distributions with standard diffusivity reduced by one third: (a) as a function of D and Z at $t = 3$ min, (b) as a function of D and Z at $t = 5$ min, and (c) depth averages for times $t = 1$, 3, 5 min

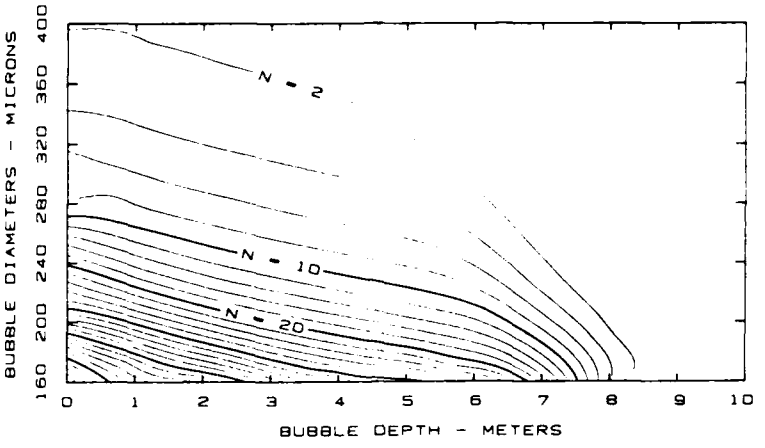

(a)

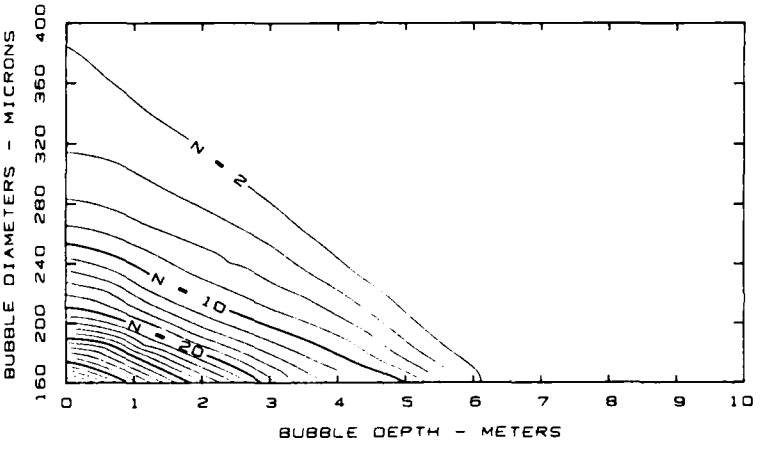

(b)

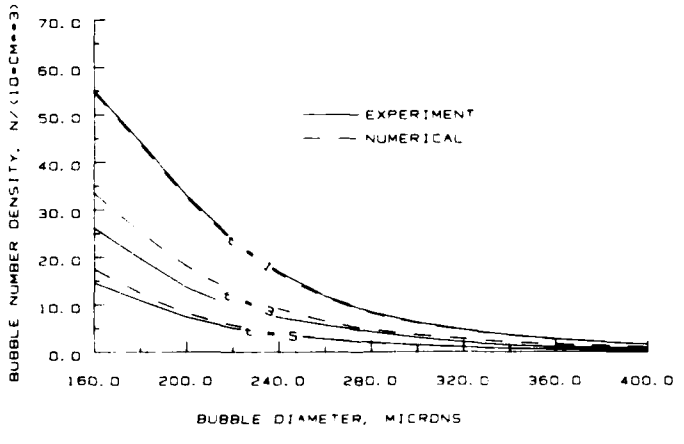

(c)

Fig. 14 — Number density distributions with standard diffusivity reduced by one third and with 1 cm/s downwash: (a) as a function of D and Z at $t = 3$ min, (b) as a function of D and Z at $t = 5$ min, and (c) depth averages for times $t = 1, 3, 5$ min

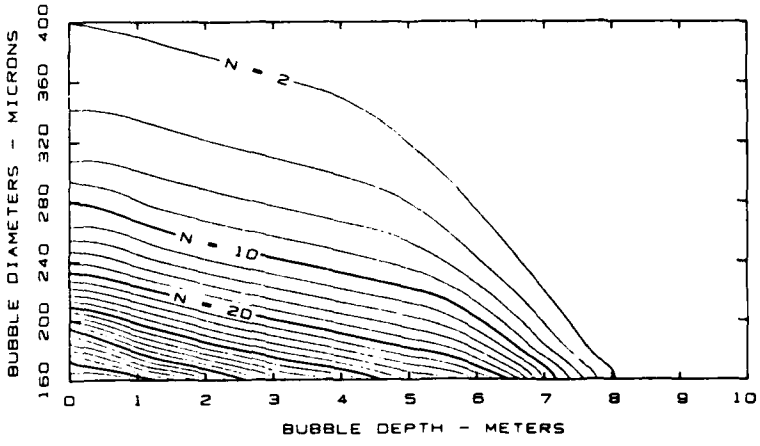

(a)

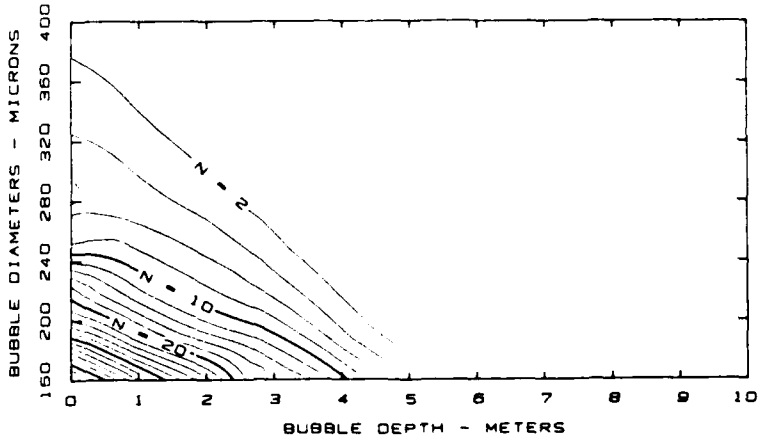

(b)

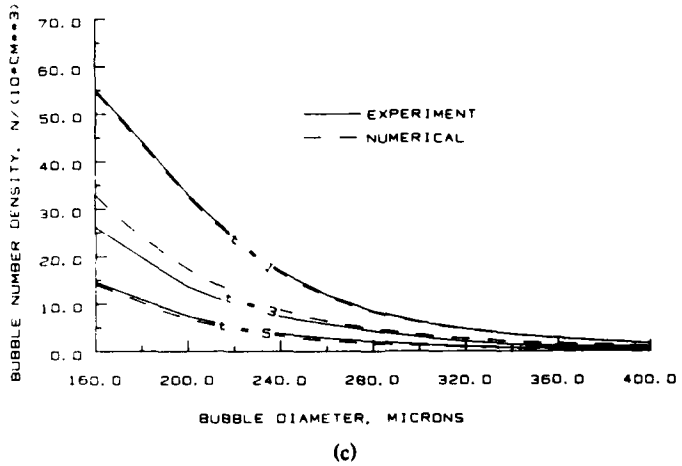

(c)

Fig. 15 — Number density distributions with standard diffusivity reduced by one third and using "dirty" bubble rise velocities: (a) as a function of D and Z at $t = 3$ min, (b) as a function of D and Z at $t = 5$ min, and (c) depth averages for times $t = 1, 3, 5$ min

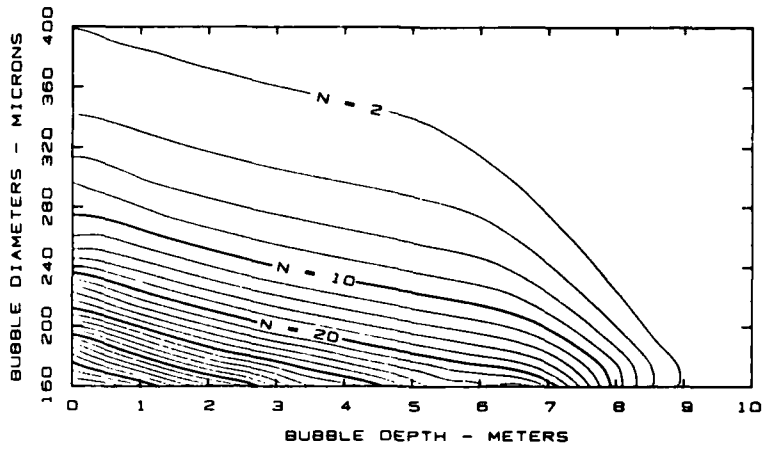

(a)

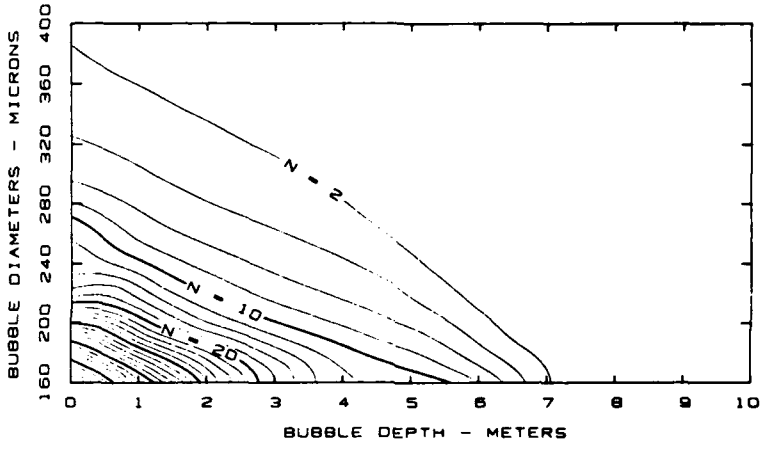

(b)

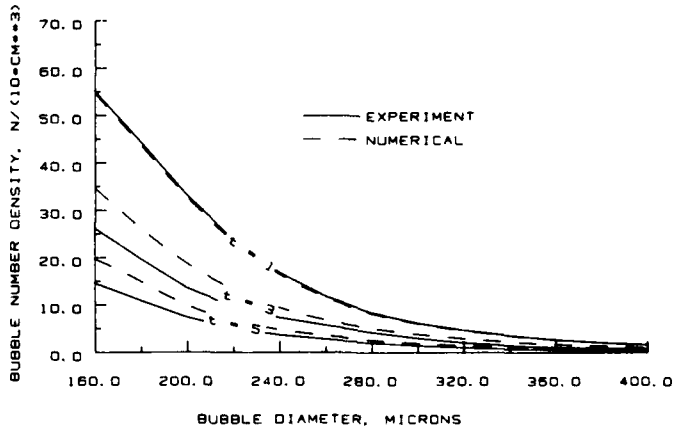

(c)

Fig. 16 — Number density distributions with standard diffusivity reduced by one third, with 1 cm/s downwash, and using "dirty" bubble rise velocities: (a) as a function of D and Z at $t = 3$ min, (b) as a function of D and Z at $t = 5$ min, and (c) depth averages for times $t = 1, 3, 5$ min

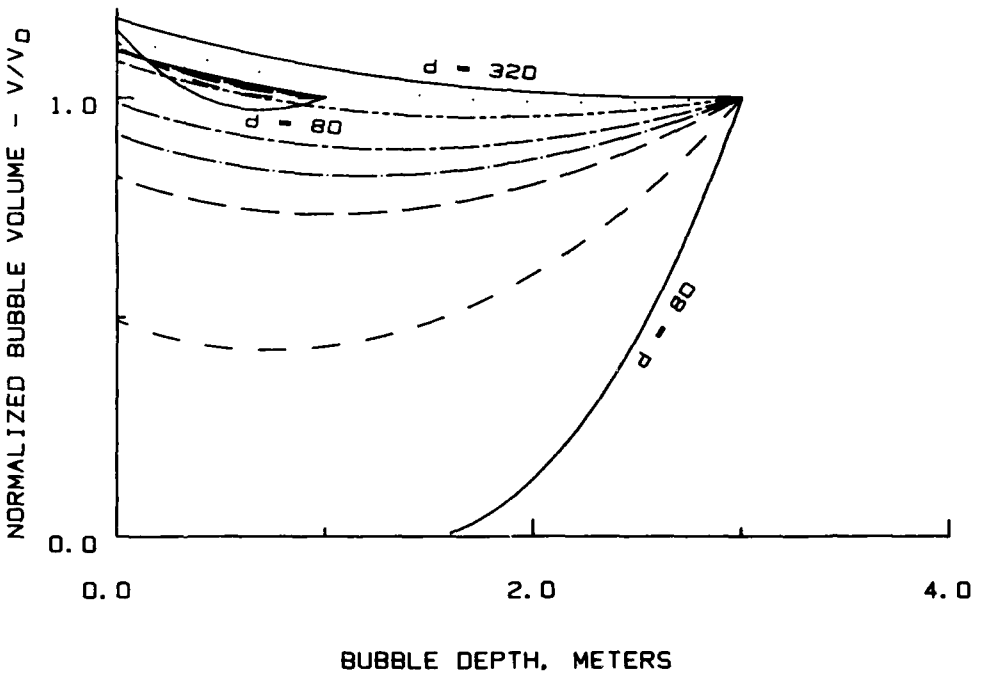

Fig. 17 — Curves of normalized volume V_n vs depth D for N_2 bubbles of diameters 80 to 320 microns showing surface layer saturation when using "dirty" bubble rise velocities

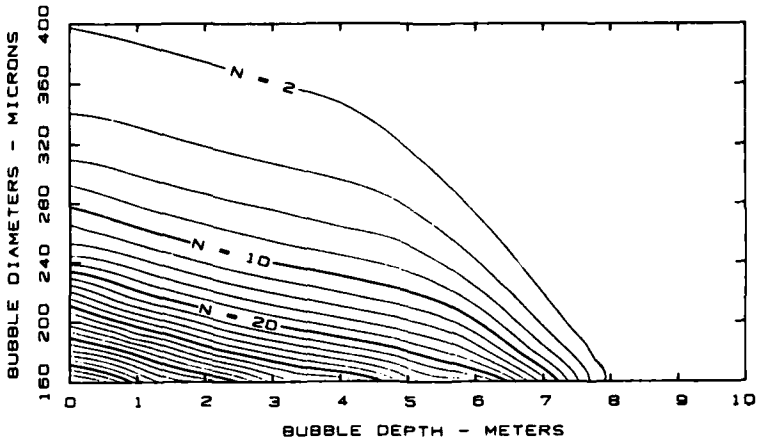

(a)

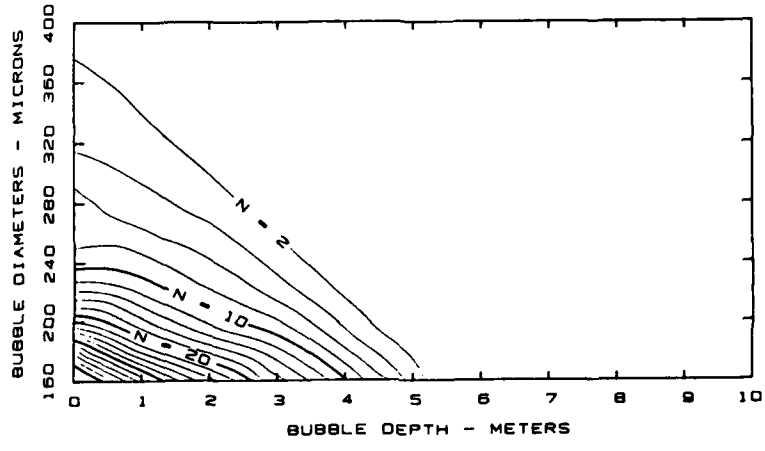

(b)

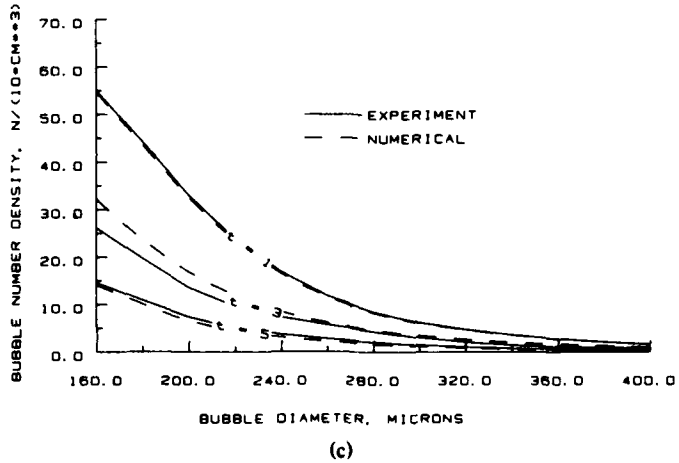

(c)

Fig. 18 — Number density distributions for O_2 - N_2 bubbles with standard diffusivity reduced by one fourth and using "dirty" bubble rise velocities: (a) as a function of D and Z at $t = 3$ min, (b) as a function of D and Z at $t = 5$ min, and (c) depth averages for times $t = 1, 3, 5$ min

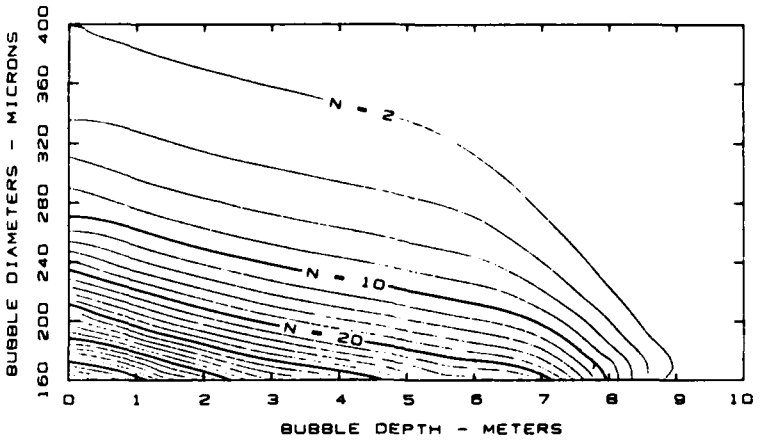

(a)

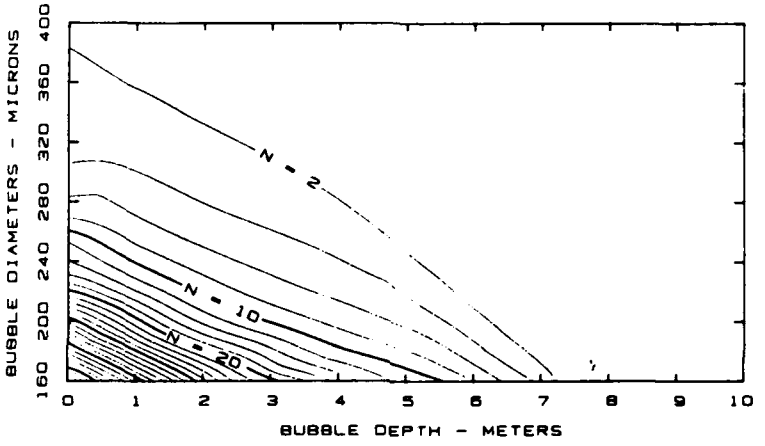

(b)

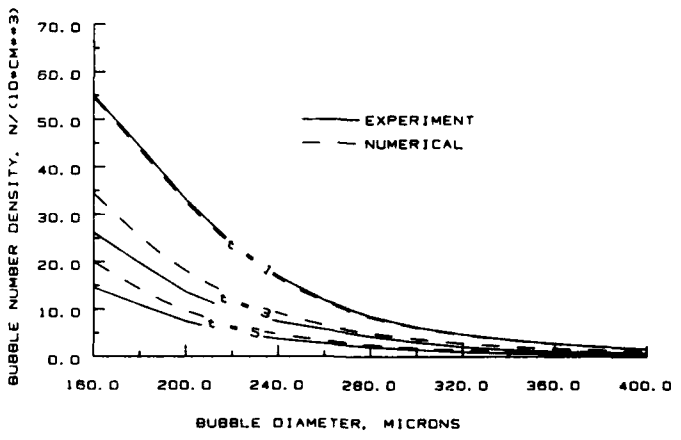

(c)

Fig. 19 — Number density distributions of O_2 - N_2 bubbles with standard diffusivity reduced by one fourth, with 1 cm/s downwash, and using "dirty" bubble rise velocities: (a) as a function of D and Z at $t = 3$ min, (b) as a function of D and Z at $t = 5$ min, and (c) depth averages for times $t = 1, 3, 5$ min

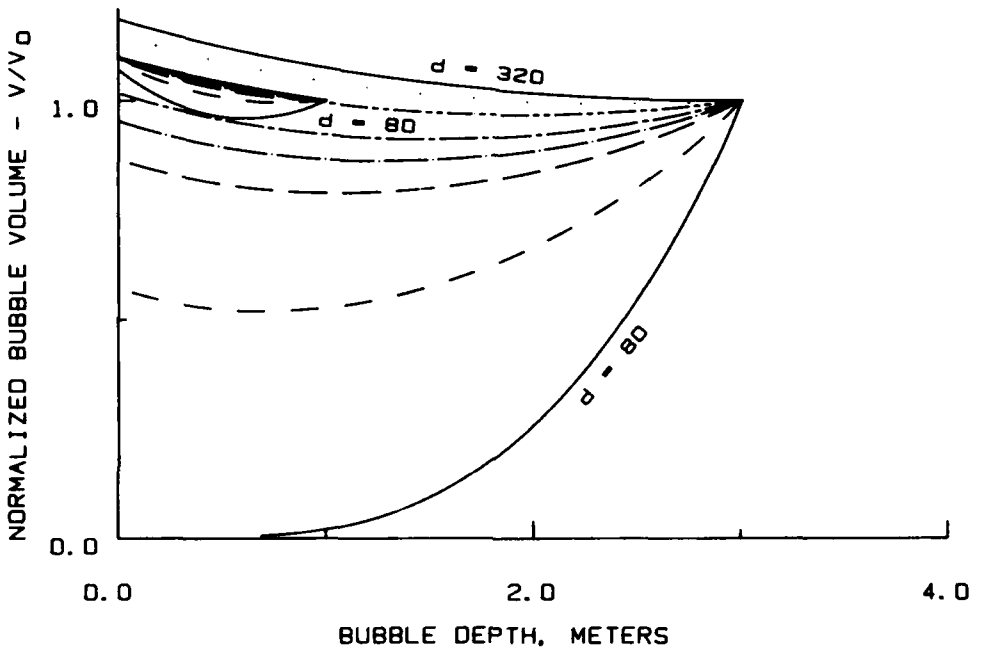

Fig. 20 — Curves of normalized volume V_n vs depth D for $O_2 - N_2$ bubbles of diameters 80 to 320 microns showing surface layer saturation when using "dirty" bubble rise velocities

SUMMARY AND CONCLUDING REMARKS

The present work on simulating bubble density distributions in seawater has given results which indicate that the discrete approach is a useful one. These results have also clearly shown that a nitrogen only model (N_2) for the bubble chemistry gives results which are comparable to those of the more complete oxygen-nitrogen model (O_2 - N_2) . Because of a number of uncertainties, this simulation model cannot be considered as completely validated in spite of the good agreement obtained between the simulation results and the experimental data. Firstly, more experimental data for number density are needed to define with more confidence the shape of the initial and downstream bubble distributions. Data at just one additional diameter (e.g. 240 μm) would help significantly. Additional data at 80 and 120 μm diameters might be adequate to fit curves with a greater degree of confidence.

A better description of "dirty" bubbles is also needed, together with more data to simulate the rise velocities of dirty or partially dirty bubbles. Also, a better specification of the diffusivity is needed in order to increase the confidence in the results of the simulation.

Other potentially significant factors in the simulation that might be considered after the "dirty" bubble uncertainties are resolved include the distribution of bubbles across the wake, the distributions of downwash throughout the wake and perhaps the effect of turbulence in the wake. Also needed is a better description of the vertical bubble distribution in the wake.

ACKNOWLEDGMENT

This work was conducted as part of a research program in free surface hydrodynamics supported by the Naval Research Laboratory.

REFERENCES

G.A. Garrettson, 1973, "Bubble transport theory with application to the upper ocean," J. Fluid Mech., Vol. 59, part 1, 187-206.

H.W. Harvey, 1960, *The Chemistry and Fertility of Sea Water*, Cambridge University Press.

R.A. Horne, 1969, *Marine Chemistry*, Wiley-Interscience, New York.

B.D. Johnson and R.C. Cooke, "Bubble populations and spectra in coastal waters: a photographic method," J. Geophysical Research, Vol. 84, No. C7, 3761-3766.

National Defense Research Committee Division 6, Summary Technical Report Volume 8, 1946, *Physics of Sound in the Sea*, reprinted 1969 as NAVMAT Report P-9675.

R.D. Peltzer, 1984, "White-Water Wake Characteristics of Surface Vessels," NRL Memorandum Report 5335.

R.H. Perry and C.H. Chilton, Editors, 1973, *Chemical Engineers' Handbook*, 5th edition, McGraw-Hill Book Co., New York.

R.A. Skop, 1984, "The Hydrodynamic Wake of a Surface Ship: Theoretical Foundations," NRL Report 8833.

S.A. Thorpe, 1982, "On the clouds of bubbles formed by breaking wind waves in deep water, and their role in air-sea gas transfer," Phil. Trans. Royal Soc. Lond. A, Vol. 304, 155-210.

R.C. Weast, Editor-in-Chief, 1965, *Handbook of Chemistry and Physics,* 42nd Edition, Chemical Rubber Co., Cleveland.